

Research Paper

Dual target gene therapy to EML4-ALK NSCLC by a gold nanoshell-based system

Siwen Li¹, Yuxi Liu¹, Yalan Rui¹, Liping Tang², Samuel Achilefu³, Yueqing Gu^{1,✉}

1. Department of Biomedical Engineering, School of Engineering, China Pharmaceutical University, 24th Tong Jia street, Nanjing 210009, Jiangsu Province, China. Phone: 86-25-83271046; Fax: 86-25-83271046.
2. Department of Bioengineering, University of Texas at Arlington, Arlington, TX, USA.
3. Department of Radiology, School of Medicine, Washington University in St. Louis, MO, USA

✉ Corresponding author: guengineering@cpu.edu.cn

© Ivyspring International Publisher. This is an open access article distributed under the terms of the Creative Commons Attribution (CC BY-NC) license (<https://creativecommons.org/licenses/by-nc/4.0/>). See <http://ivyspring.com/terms> for full terms and conditions.

Received: 2017.12.20; Accepted: 2018.02.22; Published: 2018.04.03

Abstract

Although EML4-ALK transforming fusion gene is represented in only 8% of non-small cell lung cancer (NSCLC) cases, its expression is partly responsive for the failure of current NSCLC treatments. Preventing secondary mutation of the ALK protein through direct gene manipulation could overcome NSCLC drug resistance.

Method: In this study, we developed a gold nanoshell (HAuNs) drug carrier for delivery and selective photo-thermal release of genes that target ALK and microRNA-301 in NSCLC. Additionally, the densely-coated nanoshell adsorbed high amounts of the positively-charged anticancer drug doxorubicin (DOX), generating an exciting multidimensional treatment strategy that includes gene-, thermal- and chemo- therapy.

Results: The ALK mRNA and microRNA-301 genes as the double targets exhibited the combined effect. The drug carrier system significantly improved the drug accumulation in tumor tissues due to the enhanced vascular permeability by photothermal effect, dense spherical structure and RGD peptide modification.

In vitro and in vivo results demonstrated the multiple therapeutic effects of the gold nanoshell-based system was better than the monotherapy.

Conclusion: The above results indicated the gold nanoshell-based system would be a promising translational nano-formulation platform for effective treatment of EML4-ALK-positive NSCLC.

Key words: EML4-ALK, gold nanoshell, gene therapy, hyperthermia, chemo-therapy.

Introduction

Lung cancer is the first leading cause of death among different cancer types. In the past 10 years, the morbidity and mortality of lung cancer worldwide has continued to increase, clearly becoming a major threat to public health [1]. Each year, about 1.5 million new cases of lung cancer are reported, and 80 % of these cases are diagnosed as non-small cell lung cancer (NSCLC) [2]. Among the different kinds of NSCLC, those expressing the echinoderm microtubule-associated protein-like 4-anaplastic lymphoma kinase (EML4-ALK) fusion gene mutation are among the most malignant types [3].

Approximately 8% of NSCLC patients are EML4-ALK positive, and it is estimated that approximately 70,000 new cases of EML4-ALK gene-positive lung cancer will occur all over the world in one year. [4].

EML4-ALK mutations show a strong exclusiveness in NSCLC patients, which means this kind of mutation occurs alone without mutations of other driving genes. For example, EML4-ALK fusion gene scarcely coexists with EGFR and other mutations. As a result, in the NSCLC patients expressing EML4-ALK mutations, treatment with EGFR-targeted inhibitors was associated with a poor

prognosis. Consequently, EML4-ALK fusion gene has become a unique therapeutic target for the 8% of NSCLC patients expressing EML4-ALK mutations, with great clinical significance [5]. The ALK-targeted small molecule drug crizotinib and its derivatives have shown encouraging results in the initial treatment of ALK-positive NSCLC patients. However, these ALK-targeted drugs have been shown to induce mutations of ALK kinase and increase ALK gene copy number with continuous treatment, resulting in the occurrence of drug resistance [6]. Patients treated with crizotinib or crizotinib-based drugs showed acquired drug resistance to different extents after 8 months, leading to tumor recurrence [6-8]. Gene therapy for target proteins can be an effective strategy for suppressing protein expression and can significantly improve therapeutic efficacy. Moreover, gene therapy may prevent the occurrence of secondary drug resistance caused by drug-induced mutations [9,10].

Gene therapy inhibits the expression of target proteins by suppressing the mRNA of the target protein. Small interfering RNA (siRNA) is a promising strategy to inhibit the target ALK mRNA for cancer therapy [11-13]. Takezawa et al. reported that the over-expression of ALK protein could activate both JAK/STAT3 and RAS/ERK signaling pathways to enhance expression of the anti-apoptosis gene Survivin and inhibit the tumor suppressor gene Bim, promoting the development of tumor cells in the EML4-ALK fusion mutant NSCLC [14]. Accordingly, down-regulation of ALK mRNA expression could increase the expression of Bim to induce tumor cell apoptosis. However, inhibiting ALK mRNA alone could hardly achieve an ideal therapeutic effect because intracellular protein expression is a complex process that is regulated by cross-effects of multiple signaling pathways [15]. Recently, researchers have paid much attention to the study of microRNA's function. A recent study showed that miR-301a is involved in PC progression. Lee et al. investigated aberrant miRNA expression in PC, and showed increased levels of miR-301a in PC tissues [16]. Lu et al. certified that miR-301a downregulated NF-kB-repressing factor (Nkrf) and elevated NF-kB activation [17]. Chen et al. revealed that the presence of microRNA-301 in pancreatic cancer cells down-regulates Bim expression, thereby promoting the proliferation of tumor cells [18,19]. Hence, we selected microRNA-301 as another target to amplify the treatment outcome.

In gene therapy, a specific strategy for gene transfection is indispensable to introduce foreign genes into target cells. Gold nanoshell is a novel type

of biocompatible nano-carrier, which is currently under investigation as a hyperthermia agent for cancer treatment in a phase II clinical trial [20]. The large surface area of gold nanoshell presents the opportunity to upload multiple genes and drugs simultaneously to improve therapy. The unique spatial structure formed by the densely coated spheroidal particles can prevent the biomolecules from being rapidly degraded by enzymes in the blood circulation [21-23]. Combined with the good optical-to-thermal conversion efficiency of gold nanoshell, increased temperature can break the thiol-Au bond upon NIR light irradiation, which can trigger subsequent release of the siRNAs and chemotherapeutic agents for controlled therapy [24-31]. In addition, the photothermal effect could enhance local blood perfusion and vascular permeability in tumors, resulting in improved accumulation and penetration of the gold nano-system into the tumor microenvironment [32]. Simultaneously, the surface of the gold nanoshell can be modified with tumor-targeting ligands, transforming the nano-carrier into a tumor-avid nanoparticle [33-37]. Furthermore, the dense spherical structure of the gold nano-system may facilitate its cellular uptake [38]. With the active targeting ligand RGD peptide and its dense spheroidal structure, a high concentration of HAuNs accumulated in cancer cells. Interestingly, we found that nanoshells densely coated with siRNA could absorb more of the positively charged anticancer drug doxorubicin (DOX), allowing for combinatory therapy. Concurrently, the heat caused by NIR irradiation on the gold nanoparticles could damage the tumor tissue and cells at a macroscopic level, while the gene- and chemo-therapy could inhibit the cells in a molecular level. Therefore, the treatment should exhibit a synergistic effect with the combination of gene therapy, chemotherapy and hyperthermia therapy.

Herein, we established a drug delivery system based on the gold nanoshell DOX@siRNA@HAuNs to explore an alternative effective treatment paradigm for EML4-ALK fusion mutant NSCLC. Inhibition of ALK and miR-301 exhibited a synergistic apoptotic effect on EML4-ALK cells. The drug carrier system, DOX@siRNA@HAuNs, showed many remarkable abilities, such as high drug-loading capacity, siRNA sequence protection, and tumor targeting ability. The amplified synergistic therapeutic effect was demonstrated both in vitro and in vivo, indicating the DOX@siRNA@HAuNs drug carrier system is a promising nanoplatform for EML4-ALK NSCLC treatment.

Materials and methods

Materials

Cobalt chloride hexahydrate, chloroauric acid (HAuCl₄), trisodium citrate dehydrate, and sodium borohydride were purchased from Guoyao Reagent Corporation (Shanghai, China). Dithiothreitol (DTT) and glutathione (GSH) were purchased from Sigma-Aldrich Inc. (USA). Sulfhydryl polyethylene glycol, and RGD peptide were purchased from Shanghai Sangon Biotech, Inc. EML4-ALK mutation cells H2228, normal liver cells L02 and NSCLC A549 (ALK fusion-negative, as control cells) cells were obtained from KeyGen Biotech. (Nanjing, China). Athymic nude mice were purchased from SLAC Laboratory Animal Co. Ltd. (Shanghai, China). Bovine serum albumin and cell culture media were purchased from Sangon Biotech (Shanghai) Co., Ltd. The siRNAs and nonsense sequences with or without the modification of -SH and FITC were purchased from Sangon Biological Engineering Technology & Co. Ltd. (Shanghai, China).

Synthesis of RGD @siRNA@HAuNs drug delivery system

Hollow gold nanoshells (HAuNs) were prepared by the previously reported method [23]. Stable suspensions of silver nanoparticles were synthesized in minutes using an aqueous solution of sodium citrate and silver nitrate, and the addition of sodium borohydride accelerated the chemical reaction. The reaction proceeded at 60 °C. Larger silver particles were formed from these nanoparticles by reducing additional silver nitrate in the presence of hydroxylamine hydrochloride; the nanoparticles act as nuclei for further growth. Then, the silver nanoparticles were converted into hollow gold nanoshells (HAuNs) by adding HAuCl₄ directly to the as-grown nanoparticle solution. Subsequently, multiple copies of siRNA were conjugated to the surface of the HAuNs either directly or supported by a single strand DNA linker through a quasi-covalent (Au-S) bond. Finally, moderate DOX accumulated on the surface of the prepared siRNA@HAuNs by electrostatic adsorption, forming the DOX@siRNA@HAuNs drug delivery system. The nanoparticles were stored at 4 °C. For the fabrication of the combinatory drug delivery system, Thiol-PEG-COOH was used as a stabilizer as well as a linker/spacer to attach various agents to HAuNs via one end of the thiol group. The amino group of the targeting peptide RGD was coupled with the carboxyl group of thiol-PEG-COOH (amount ratio RGD/PEG=1:1) through EDC reaction catalyzed by NHS.

Nucleic acid electrophoresis assay of siRNA protection

To investigate the protective effect of siRNA@HAuNs, delivery vectors were incubated with 0.25% RNase A for 0.5 h. Then, the sample was loaded on a 1% agarose gel containing 0.01% Gel-Red and run at 90 V for 30 min. To release the loaded siRNA, the samples were treated with heparin at a dose of 1 U/mg siRNA in DEPC-treated water.

Endosomal escape of siRNA

Approximately 3×10⁵ H2228 cells were seeded onto confocal dishes and incubated overnight at 37 °C. Cells were then treated with siRNA@HAuNs (siRNA with FITC). After incubation for 4 h, Lyso-Tracker Red was added and incubated for 0.5 h. Then, the intracellular fluorescence was visualized using confocal laser scanning microscopy (CLSM).

Laser-induced DOX release

Approximately 3×10⁵ H2228 cells were seeded onto confocal dishes and incubated overnight at 37 °C. Cells were then treated with RGD@DOX@HAuNs (siRNA without FITC) and imaged before or after laser treatment (785 nm light irradiation, 1.2 W/cm², for 5 min). After incubation for 4 h, Hoechst was added and incubated for 0.5 h. Then, the intracellular fluorescence was visualized using CLSM.

In vitro therapeutic effect

Cellular toxicity of nanoshells and the DOX@siRNA@HAuNs drug delivery system in different cell lines and conditions was measured by MTT assay. Cell apoptosis caused by the DOX@siRNA@HAuNs drug delivery system with 785 nm laser was detected by flow cytometry and LCSM.

In vivo therapeutic efficacy

All animal experiments were carried out in compliance with the Animal Management Rules of the Ministry of Health of the People's Republic of China (document NO. 55, 2001) and the guidelines for the Care and Use of Laboratory Animals of China Pharmaceutical University. Nude mice bearing H2228-derived tumors were randomly assigned to 1 control group and 5 experimental groups (n=5) when the tumor diameter reached 0.5 cm. Mice in the control group were injected with PBS while the experimental groups were injected with DOX, bare nanoshells and DOX@siRNA@HAuNs. 12 h post-injection, different therapeutic schedules were performed on each experimental group: (1) Dox injection without light irradiation; (2) 785 nm light irradiation (1.2 W/cm²) for 5 min with nanoshell injection; (3) 785 nm light irradiation (1.2 W/cm²) for 5

min with DOX@siRNA@HAuNs. Tumor sizes and body weights were measured every other day. Tumor volumes were measured using calipers and calculated according to the following formula: size (mm³) = length (mm) × width (mm)²/2. All mice were sacrificed and the tumors were collected 14 days after treatment.

Results and discussion

Function of ALK siRNA and miRNA-301 inhibitor in H2228 cells

We used western blot to confirm the function of the double gene therapy targeting ALK and miRNA-301 in H2228 cells. Treatment of the cells with ALK siRNA significantly down-regulated the expression of ALK and the phosphorylation level of downstream protein p-ERK in H2228 cells, inhibiting cell proliferation (**Figure 1A**). In addition, ALK siRNA increased the expression of apoptotic protein Bim. The results also showed that the miRNA 301 inhibitor improved Bim expression, while miRNA 301 mimics suppressed Bim activity in H2228 cells. Interestingly, the ALK siRNA treatment had little or no influence on Bim expression in A549 cells where the ALK level was in the normal range (**Figure 1B**). These results indicate that the effect of ALK siRNA is cell-dependent and the ALK siRNA-based treatment would be specific. In addition, both ALK siRNA and miRNA 301a inhibitor are able to increase the expression of Bim in H2228 cells. Therefore, simultaneous inhibition of the dual-targets, ALK mRNA and miRNA 301a, could exert a synergistic effect on the survival of EML4-ALK fusion mutation lung cancer. We compared the cell viability of EML4-ALK mutation H2228 cells and ALK fusion-negative A549 cells after siRNA transfection with Lipofectamine (**Figure 1C**). We found that the cell viability of H2228 cells (33.1%) was much lower than that of A549 (81.3%) when the cells were incubated together with ALK siRNA and microRNA-301 ($p < 0.05$). This finding suggests that the double target gene therapy amplified its therapeutic effect in cancer cells. The fact that the normal NSCLC A549 cells survived over 80% in each group indicates that this combination therapy is selective to cancer cells expressing higher levels of EML4-ALK mutation than ALK fusion-negative cells.

We next postulated that apoptosis induction may mediate the cytotoxic effect of the combination therapy. To test this hypothesis, the extent of cell apoptosis following different treatments was analyzed using flow cytometry (FCM). After simultaneously transfecting cells with both siRNAs, the apoptosis rate of H2228 cells increased to 44.1%, which was higher than the effects of ALK siRNA

(25.7%) or microRNA-301 (25.1%) alone (**Figure 1D-E**). The ensemble of these results lends strong support to the development of a dual gene targeting strategy for treating EML4-ALK NSCLC.

Synthesis and Characterization of RGD@siRNA@DOX@HAuNs drug delivery system

The structure of RGD@siRNA@DOX@HAuNs and the mechanism of target selection are illustrated in **Scheme 1**. The transmission electron microscopy (TEM) image of the prepared RGD@siRNA@DOX@HAuNs (**Figure 2A**) shows a core-shell structure of the drug carriers. The mean hydrated diameters of the nanoshell and the sequence-coated shell are ~25 nm and ~35 nm, respectively (**Figure S1A-B**) and the PDI value was ~0.06. Analysis of the photothermal conversion showed that laser irradiation can quickly and significantly increase the temperature from 25 °C to ~53 °C within 5 min (**Figure 2B**).

The UV-visible absorption spectra of various components (**Figure S1C**) confirmed the successful conjugation of siRNA (absorption peak @215 nm), DOX (absorption peak @480 nm), and HAuNs (absorption peak @800 nm), with a Zeta potential of -13 mV for HAuNs (**Figure S1D**). Modification of the positively charged RGD peptide slightly changed the Zeta potential to -12 mV. In particular, uploading the negatively charged siRNA greatly enhanced the negative potential (-20 mV), favoring enhanced adsorption of the positively charged anticancer drug DOX. The siRNA was loaded onto the HAuNs by Au-S bonds, not by electrostatic adsorption, so the negative potential would not hinder uploading of siRNA in this study. The fluctuation in Zeta potential indicates the success of each reaction process and production of the novel drug delivery system RGD@siRNA@DOX@HAuNs.

The correlation of siRNA loading with DOX adsorption was also investigated. We found that nanoshells with increased coating of negative siRNA sequence (siRNA@HAuNs) could adsorb more DOX, with a maximum of 20% DOX loading (the amount of DOX was calculated by the ultraviolet absorption spectrum of DOX in the solution). At low concentrations, there was a linear relationship between the loading quantities of siRNA and DOX. Specifically, we found that the optimal siRNA loading concentration to achieve 20% of DOX loading was 200 nM (**Figure 2C**). The laser-triggered release of RGD@DOX@siRNA@HAuNs as a whole was analyzed at different illumination times (**Figure 2D**). Within 5 min of laser light exposure, there was a linear relationship between laser duration (minutes) and cumulative drug release (%). In addition, a 5 min

light exposure was sufficient to trigger the release of over 80% of siRNA and DOX, indicating that drug release from the HAuNs drug carrier could be controlled by light illumination.

The stability and drug release properties of HAuNs before and after PEG coupling were characterized at different pH values and different concentrations of salt solution (Figure S2A-D). The

results show that the cumulative drug release of both siRNA and DOX were low under different conditions, with the exception of DOX release in acidic environments. This unique property might enhance drug release in the tumor microenvironment, which is known to be more acidic than surrounding tissue (pH value : blood and healthy lung tissue 7.35~7.45; tumor lung tissue 6.5~7.0).

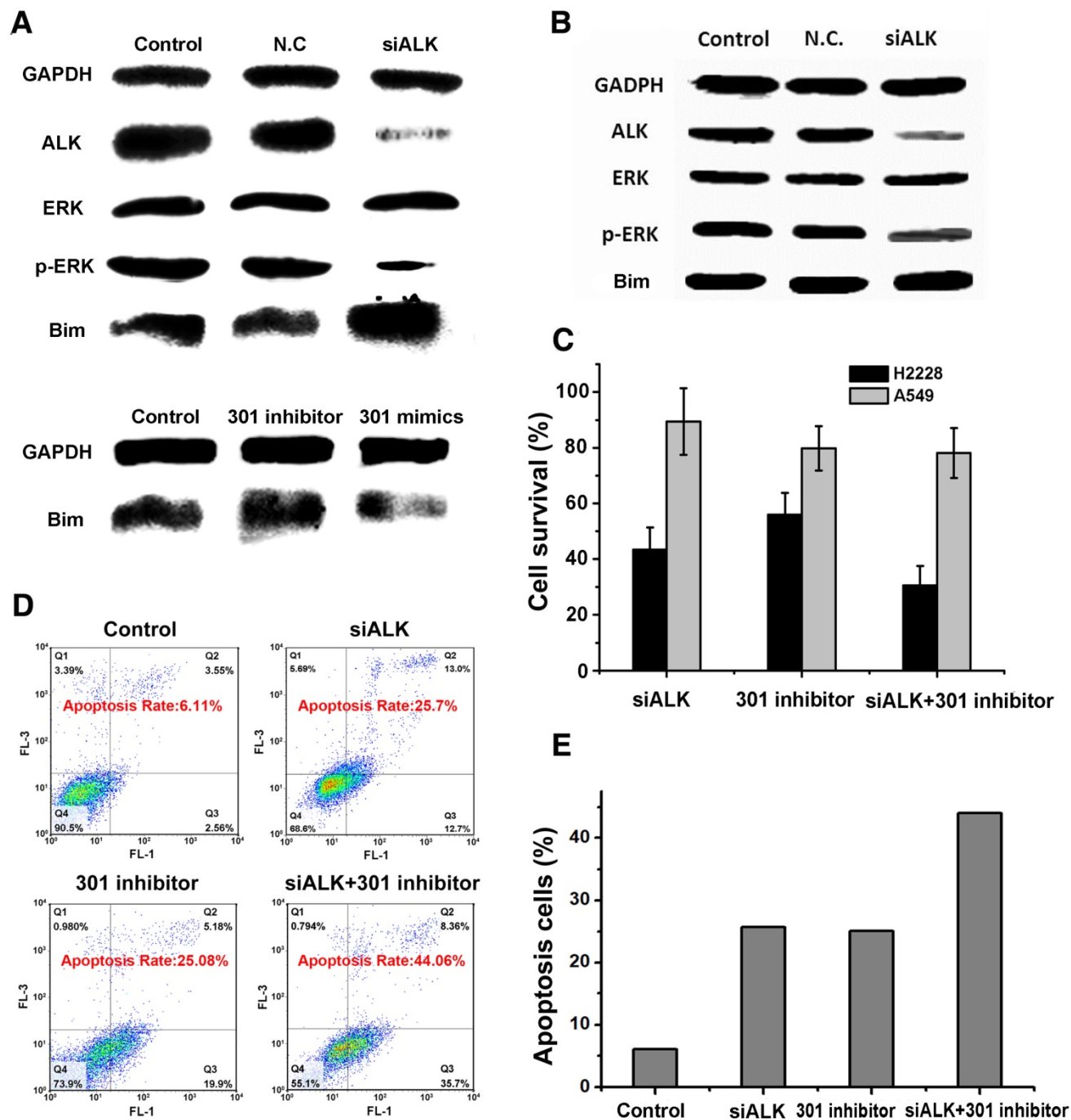
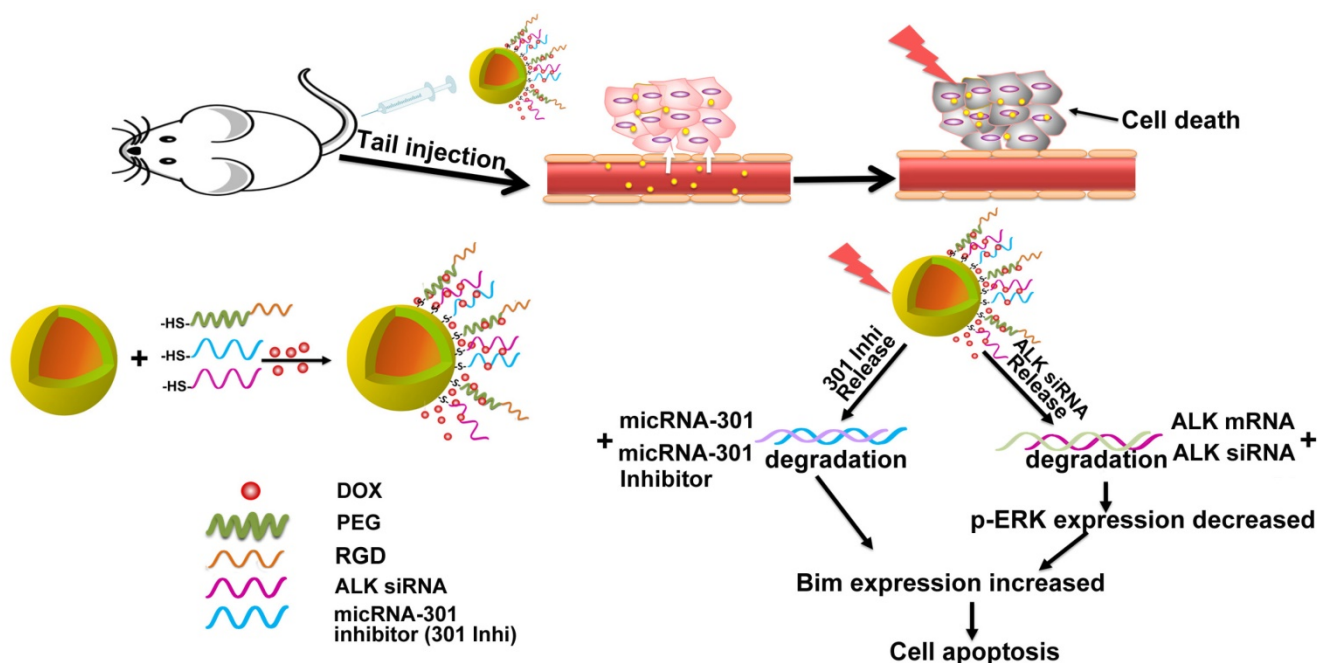


Figure 1. The mechanism of treatment target selection and the synergistic effect of gene silencing. (A) Western blot assay after ALK siRNA, miR-301 inhibitor and miR-301 mimics transfection in H2228 cells. (B) Western blot assay after ALK siRNA transfection in A549 cells. (C) Survival of cells treated under the conditions in (A-B) determined by MTT assay. (D) Apoptosis of cells treated under the above conditions assayed by AV-PI kit. (E) Quantitative analysis of (D). Data are given as mean ± SD (n=5). *, P<0.05.



Scheme 1. Schematic illustration of the nanostructure design and the target selection mechanism of gene therapy.

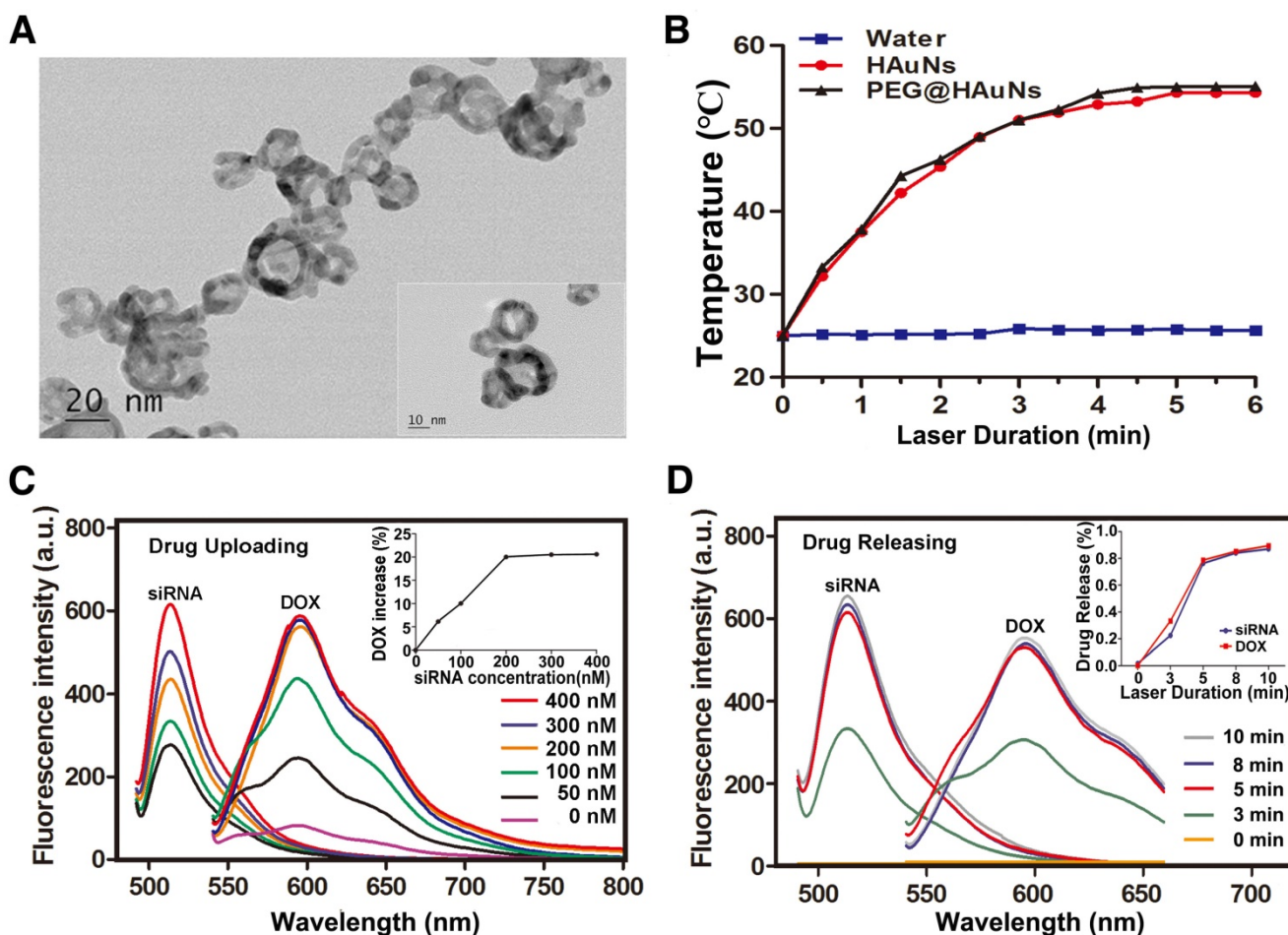


Figure 2. Characterization of the RGD@siRNA@DOX@HAuNs drug carrier system. **(A)** Transmission electron microscopy (TEM) characterization of the drug carrier system. **(B)** The photothermal conversion of HAuNs with NIR laser irradiation **(C)** Relationship between the amount of conjugated siRNA and DOX adsorption (siRNA-FITC: 520 nm, DOX: 585 nm). **(D)** Relationship between drug release and light irradiation time (siRNA-FITC: 520 nm, DOX: 585 nm). Data are given as mean ± SD (n=5). *, P<0.05.

Properties of the RGD@DOX@siRNA@HAuNs drug delivery system

siRNA sequence protection ability

The nucleic acid electrophore diagram (Figure 3A) depicts the stability of siRNA in a solution of the hydrolytic enzyme (Rnase 1). siRNA and siRNA@HAuNs exhibited bright spots in the electrophore lane (lane a\|b) without Rnase 1 incubation. When ALK siRNA itself was incubated with Rnase 1, no signal was detected in the lane, implying complete degradation of the siRNA. However, upon attachment of ALK siRNA to the HAuNs, a bright signal was observed in the Rnase 1 and serum solution, indicating that the nanoshell protected the coated siRNA. As expected, the siRNA sequence was

detached from the shell after NIR irradiation and degraded by the Rnas I enzyme, leading to disappearance of the signal in the electrophore lane. These results support the siRNA protective ability of the HAuNs carrier.

Improved transfection efficiency

Figure 3B shows a comparison of the gene transfection efficiency of HAuNs and the widely used commercial Lipofectamine reagent Lip2000. After incubation with siRNA@HAuNs, the expression of ALK in H2228 cells was significantly suppressed (28.8%), while it remained at 41.2% with Lip2000 transfection ($p < 0.05$). The results indicated that HAuNs are an ideal siRNA vector with better gene transfection efficiency than Lipofectamine.

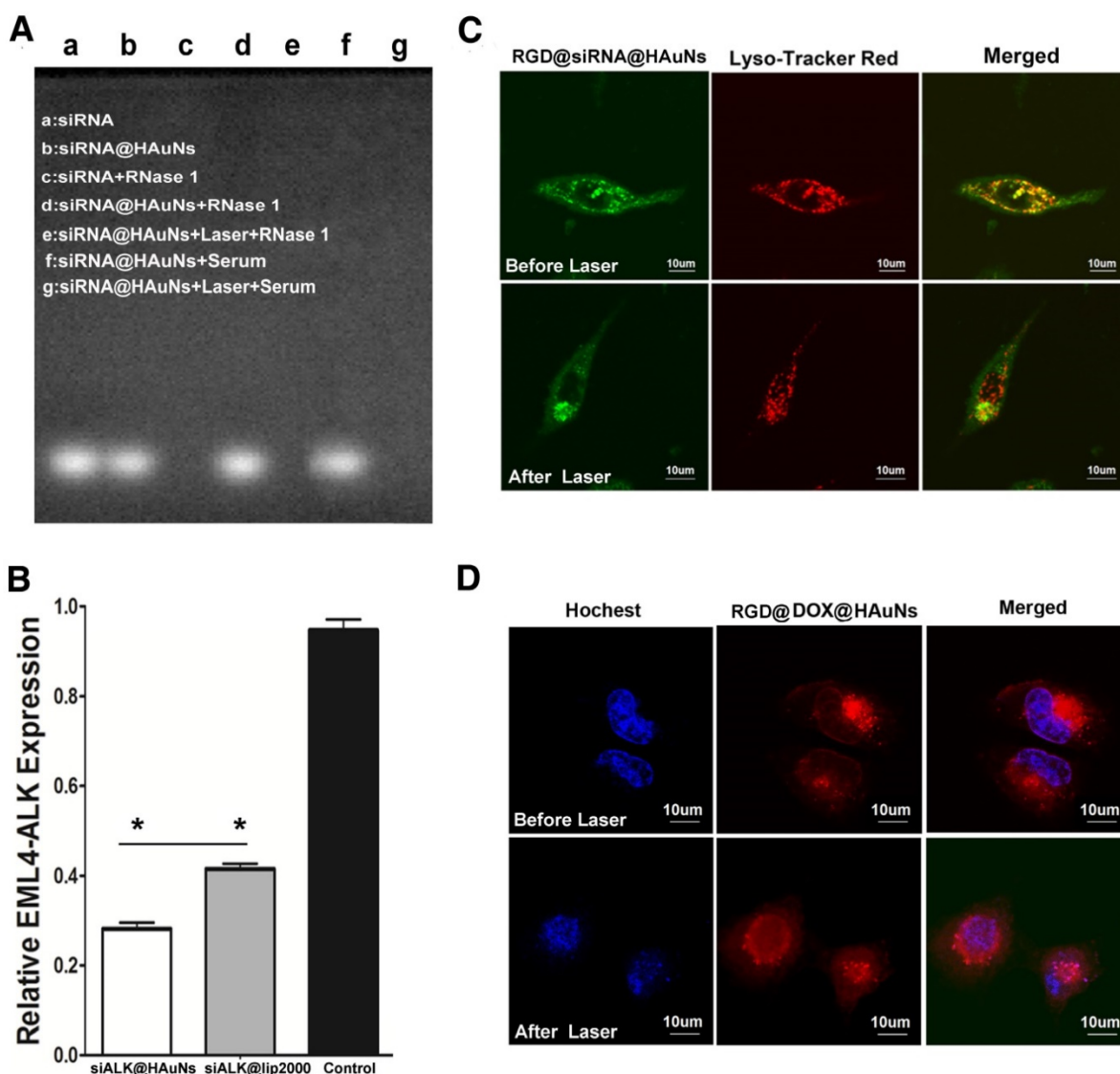


Figure 3. The properties of the RGD@siRNA@DOX@HAuNs drug carrier system. (A) The nucleic acid electrophore diagram for various conditions. (B) Relative mRNA expression of EML4-ALK determined by real-time PCR. (C) Laser confocal microscopy image of endosomal escape of RGD@siRNA@DOX@HAuNs before and after laser illumination; red: lysosome, green: siRNA-FITC, and yellow: colocalization of siRNA-FITC and endolysosome. (D) Laser confocal microscopy image of DOX release after laser illumination; red: DOX, blue: hochest. Data are given as mean \pm SD (n=5). *, $P < 0.05$.

Endosomal escape

The localization of siRNA@HAuNs in H2228 cells was imaged by confocal microscopy (**Figure 3C**). Before NIR irradiation, the siRNA@HAuNs (green fluorescence) were well colocalized with endosomes (red fluorescence), indicating that siRNA@HAuNs are in the endosomal compartment. However, after NIR irradiation, the green fluorescence separated from the red, suggesting that siRNA@HAuNs escaped from the endosome, supporting the endosomal escape ability of HAuNs with laser-induced heat generation. It is known that nanoparticles may initially enter the endosome after cell uptake and then be transferred to the lysosome, where the particles and loaded drugs are degraded. To avoid this fate, the nano-carriers should be designed to quickly escape from lysosomes to allow the effective drug to reach the target. For this nanoshell-based drug system, NIR irradiation induced photothermal effects, leading to permeabilization of endosomes by the increased temperature.

DOX release

To further explore the control of DOX release from the drug delivery system, DOX@siRNA@HAuNs were irradiated at the cellular level using a laser confocal microscope (**Figure 3D**). DOX and nuclear dye fluorescence were false-colored red and blue, respectively. The result shows that the red and blue fluorescence did not overlap without irradiation, indicating that DOX did not enter the nucleus because most DOX was adsorbed onto DOX@siRNA@HAuNs. However, after light treatment, drug release was evidenced by red and blue fluorescence overlap, showing that a large amount of DOX was released from DOX@siRNA@HAuNs and entered the nucleus. These results also confirmed that DOX release can be achieved by 785 nm laser irradiation. The reason that DOX could be released by laser irradiation is mainly by the breakage of siRNA from HAuNs (Au-S) and HAuN collapse, which leads to a change in electric potential [25,26].

Tumor-targeting ability of the RGD@DOX@siRNA@HAuNs drug delivery system

Figure 4A compares the cellular uptake of the nanoshell system with and without RGD modification. RGD peptide conjugation was found to significantly improve the efficiency of drug uptake by H2228 cells. At a similar incubation time (30 min), the RGD-modified group showed stronger green fluorescence (FITC-labelled siRNA) than the non-RGD group. Quantitative analysis of HAuNs-associated fluorescence intensities demonstrated that the RGD conjugation significantly increased ($p < 0.05$)

the cellular uptake of the drug delivery system (more than double growth) (**Figure 4B**). For further evaluating the cellular uptake of gold nanoparticles coated with different components, dark field microscopy was performed. The intensity of white light represents the amount of nanoparticle in the cells (**Figure 4C**). As anticipated, RGD@siRNA@HAuNs-treated cells exhibited the strongest light signal in cells compared to the weakest and low signals found in free HAuNs- and siRNA@HAuNs-incubated cells. This result confirmed that siRNA coating could enhance the cell uptake of the nanoparticles and that the RGD peptide conjugation can further improve the cell targeting capability of siRNA@HAuNs. Further, inductively coupled plasma-mass spectrometry (ICP-MS) was applied to quantitatively determine the elemental gold content in the H2228 cells (**Figure 4D**). The intracellular content of Au was 3×10^4 /per cell for HAuNs incubation, 1×10^5 /per cell for siRNA@HAuNs-treated cells and 6×10^5 /per cell for RGD@siRNA@HAuNs-treated cells. The quantitative ICP-MS results were consistent with the results of dark field microscopy, further validating the enhanced targeting efficiency provided by the RGD peptide.

To investigate the bio-distribution and tumor-targeting ability of RGD@DOX@siRNA@HAuNs in vivo, near-infrared fluorescence imaging was performed in H2228 tumor-bearing nude mice. MPA, a hydrophilic near-infrared fluorescence dye with similar molecular weight as DOX, was used to replace the DOX for NIR imaging. We found that RGD@MPA@siRNA@HAuNs distributed throughout the body within 30 min, then gradually accumulated in the tumor site up to 12 h post-injection (**Figure 4E**). As expected, no fluorescence signal was observed at the tumor site in the MPA administration group. The result demonstrated the favorable tumor-targeting ability of the nanoshell-based drug carrier system. For exploring the blood perfusion of tumor tissues upon photothermal stimulation, the H2228 tumor bearing mice with different treatments were sacrificed and the tumor sections were analyzed by hematoxylin and eosin (H&E) staining (**Figure 4F**). The blood perfusion and extravasation were elevated upon laser irradiation of the gold nanoshells, confirming the enhanced blood permeability via thermal effects. In contrast, less blood signal was observed in the group without laser exposure. The data suggest that additional antitumor drug will be effectively delivered to the cancerous tissue through the blood stream after NIR irradiation. To further investigate the tumor delivery abilities, histological sections of different organs (tumor, heart, liver, spleen, and kidney) were analyzed by confocal microscopy. As seen in **Figure 4G**, free DOX distributed in all the

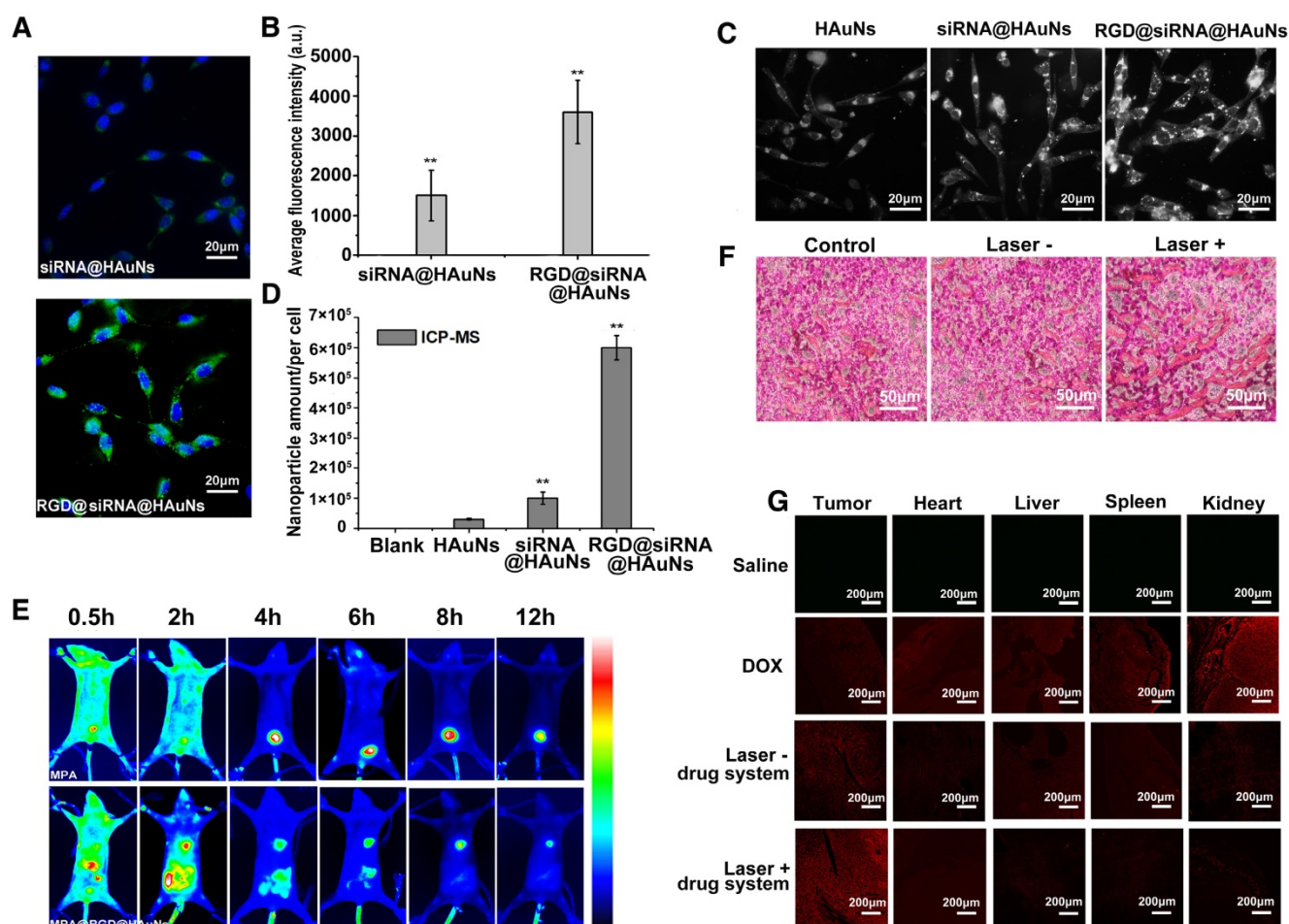


Figure 4. The tumor-targeting ability of the RGD@siRNA@DOX@HAuNs drug carrier system. (A) Laser confocal microscopy images of the cell-uptake ability of the nano-carrier with or without RGD modification; green: siRNA-FITC, blue: Hoechst. (B) The quantification of the laser confocal microscopy images in (A). (C) Dark field microscopy images of H2228 cells with HAuNs, siRNA@HAuNs and RGD@siRNA@HAuNs incubation. (D) ICP-MS assay of HAuNs, siRNA@HAuNs and RGD@siRNA@HAuNs in H2228 cells. (E) NIR images of MPA and RGD@siRNA@MPA@HAuNs dynamics in H2228 tumor-bearing nude mice at different times after intravenous injection. (F) H&E stained sections of H2228 tumors after RGD@siRNA@MPA@HAuNs treatment and laser irradiation; Laser-: treatments without NIR laser irradiation; Laser+: treatments with NIR laser irradiation. (G) Laser confocal microscopy images of tissue samples of tumor, heart, liver, spleen and kidney from different treatment groups; red: fluorescence of DOX. Data are given as mean \pm SD (n=5). *, P<0.05.

organs, indicating the potential for severe toxicity to normal organs. For mice administrated with the RGD-modified nanoshell system, strong DOX signal was observed in the tumor tissue, while low signals were exhibited in other tissues. These results show that the RGD@DOX@siRNA@HAuNs have high affinity to tumor tissue. Moreover, the tumor accumulation of DOX was greatly improved by the laser irradiation, confirming the enhanced permeability of the tumor blood vessels by the photothermal effect and reduced accumulation of nano-drugs in other vital organs.

In vitro therapy of RGD@DOX@siRNA@HAuNs

To investigate the cell toxicity of the HAuN itself, a range of concentrations of HAuNs was cultured with H2228 (Figure 5A). The results showed that the H2228 tumor cells and L02 normal cells did not exhibit obvious cytotoxicity until the

concentration of HAuNs exceeded 1.5 nM, which was used in further studies.

The laser duration (illumination time) is an important factor for this treatment. To identify the optimal treatment time, different illumination time gradients were tested with RGD@DOX@siRNA@HAuNs, and the HAuNs were used as control group. The results revealed that within 5 min irradiation, the cell survival rate of the two groups were 23% and 47% (Figure 5B) (p<0.05). Interestingly, beyond 5 min irradiation, there was no obvious additional impact on the cell survival. Thus, 5 min was the optimal time for the therapy. Equally important, the treatment effect of the RGD@DOX@siRNA@HAuNs group was obviously better than that of the HAuNs group after laser irradiation (cell survival rate less than double reduce, p<0.05).

The therapeutic efficacies between single treatment and combined treatment were also

compared in our study (Figure 5C). Using an *in vitro* model, we found that the cell survival rate of each group was 42% (HAuNs+Laser), 36.5%(DOX), and 20% (RGD@DOX@siRNA@HAuNs). These results confirmed our hypothesis that the combined group (compared with the single treatment: photothermal induced by HAuNs, DOX, siRNA effect in figure 1C) displayed the best treatment effect through a multidimensional cooperative treatment effect that includes hyperthermia, chemotherapy, and gene therapy.

The ability of drug carriers to induce cell apoptosis was also evaluated using a AV-PI kit (Figure 5D). Flow cytometry results showed that the apoptosis rate of the RGD@DOX@siRNA@HAuNs group reached 69.1%, while that of the HAuNs group was only 0.267%. Further, confocal microscopy (Figure 5D) revealed that most cells were already in

the late stage of apoptosis (red and green colors represent the cells in the stage of apoptosis) after treatment by RGD@DOX@siRNA@HAuNs + Laser, indicating the excellent therapeutic efficacy of RGD@DOX@siRNA@HAuNs at the cellular level. The cell apoptosis rates caused by each monotherapy (only ALK siRNA or only micRNA-301 inhibitor) were less than the designed final drug system (Figure S3).

Using Calcein-AV and PI to stain live and dead cells, respectively, we show that most of the cells treated with laser or HAuNs were not damaged (Figure 5E). In contrast, the cells within the semicircle dashed line (Figure 5Ed) were almost dead under the HAuNs and laser treatment, while cells in the unexposed area outside the semicircle were still alive. This confirmed the role of HAuNs hyperthermia in inducing apoptosis.

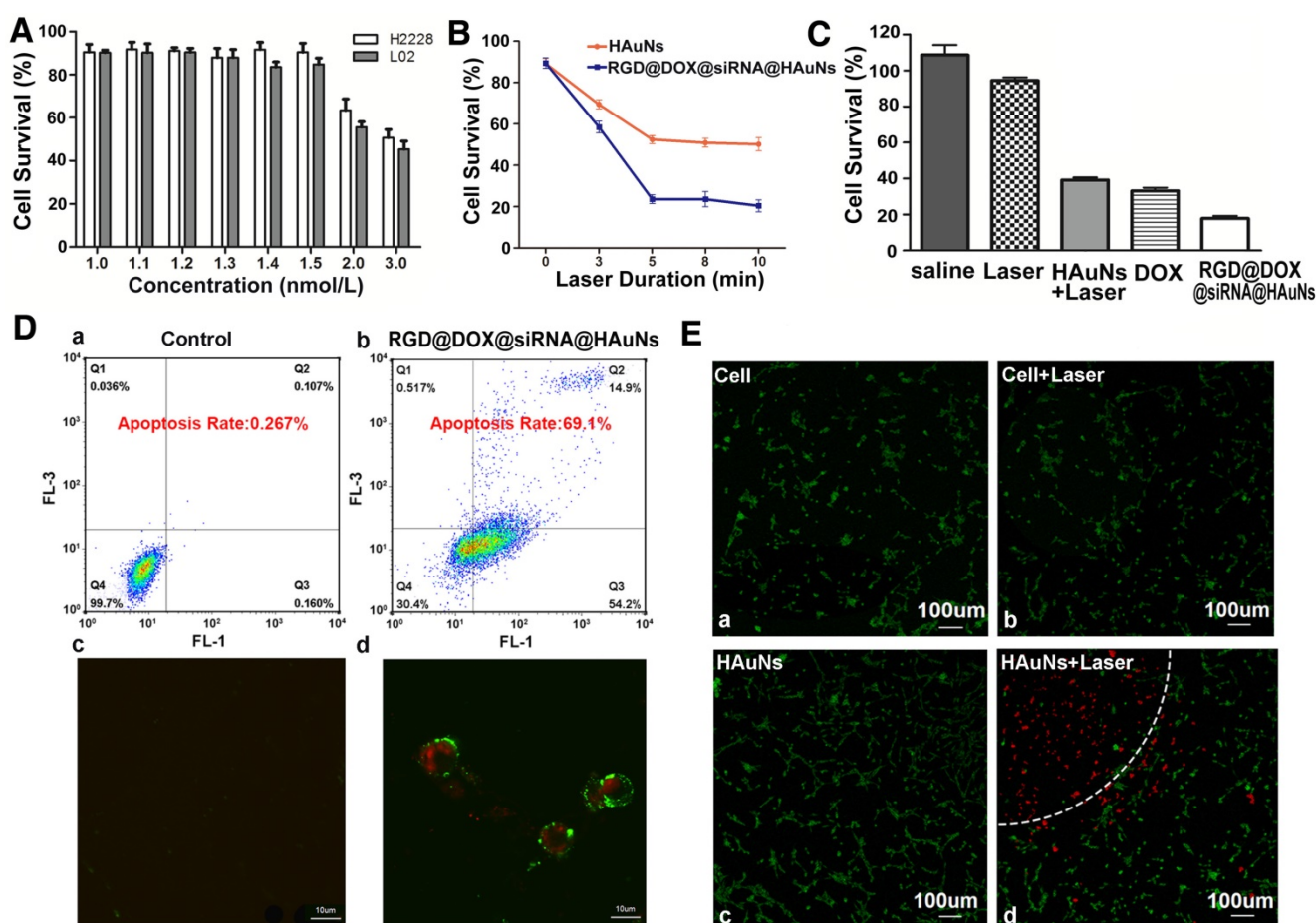


Figure 5. Treatment efficacy of RGD@siRNA@MPA@HAuNs at a cellular level. (A) Survival rate of H2228 cells and L02 cells after incubating with different concentrations of bare HAuNs. (B) Survival rate of H2228 cells after incubating with bare HAuNs and RGD@siRNA@MPA@HAuNs with different laser duration times. (C) Survival rate of H2228 cells treated under the above conditions determined by MTT assay. (D) Flow cytometry and laser confocal microscopy examination of the apoptosis of H2228 cells after irradiation of RGD@siRNA@MPA@HAuNs. (E) Laser confocal microscopy of photothermal therapy of HAuNs in H2228 cells; viable cells were stained green with Calcein-AV, and dead cells were stained red with PI. Cells were treated with only the dye (a) as the control group, HAuNs without irradiation (b), irradiation only (c) and HAuNs with irradiation (d). Data are given as mean ± SD (n=5). *, P<0.05.

In vivo antitumor therapeutic efficacy of RGD@DOX@siRNA@HAuNs

The in vivo antitumor efficacy of RGD@DOX@siRNA@HAuNs was further evaluated in a nude mouse model (H2228 cells subcutaneous transplantation tumor). The tumor growth rate, survival rate and the body weight of the mice under different treatments were monitored (Figure 6). Tumors in the control mice treated with saline grew faster than the treated groups (Figure 6A-C). The RGD@DOX@siRNA@HAuNs treatment group exhibited the optimal inhibition effect of tumor growth. The growth of H2228 tumor was inhibited at a rate of 65% after the administration of RGD@DOX@siRNA@HAuNs+ laser, which is higher than that of the free HAuNs + laser (43%) and free DOX (45%) groups. Furthermore, the weight of mice bearing H2228 tumors in the RGD@DOX@siRNA@HAuNs group was stable compared with the DOX- and HAuNs-treated groups (Figure 6D). The 22-day survival rate of mice in the RGD@DOX@siRNA@HAuNs group was 80%, a much better outcome than the free HAuNs (40%) and free DOX (40%) groups, whereas all the mice in the saline group died by day 16 (Figure 6E). These results demonstrate the efficacy of multimodal nanoparticle over the over the free DOX and photothermal (free gold nanoshell) was realized by the RGD@DOX@siRNA@HAuNs drug carrier system.

To further investigate toxicity on the major organs of mice and the anti-tumor effects of the different treatments, histological examination was conducted. The results showed that the number of tumor cells in the saline-injected group was significantly higher than that in the other two groups (Figure 6F). The tumor cells were in a dense mitotic condition, suggesting that the tumor cells were primed for continued rapid proliferation. Histopathological examination of tumor tissues in the RGD@DOX@siRNA@HAuNs-treated group revealed more pronounced pathological changes than that of the DOX-treated group. Clearly, the tumor treatment efficacy of RGD@DOX@siRNA@HAuNs is superior to that of free DOX in this study. Meanwhile, the DOX-injected group showed more severe cardiotoxicity, liver toxicity and renal toxicity. In contrast, the organ toxicity in the RGD@DOX@siRNA@HAuNs group was mild. The reason for this observation can be attributed to the tumor-targeting drug carrier system that efficiently delivered and retained more drugs (DOX and siRNA) in the tumor tissue in vivo, thereby enhancing the treatment efficacy with minimal side effects. Finally, the ALK and Bim expressions in the tumor tissue (RGD@DOX@siRNA@HAuNs) were tested, and the results exhibited that the expressions of ALK and Bim could be inhibited effectively (Figure S4).

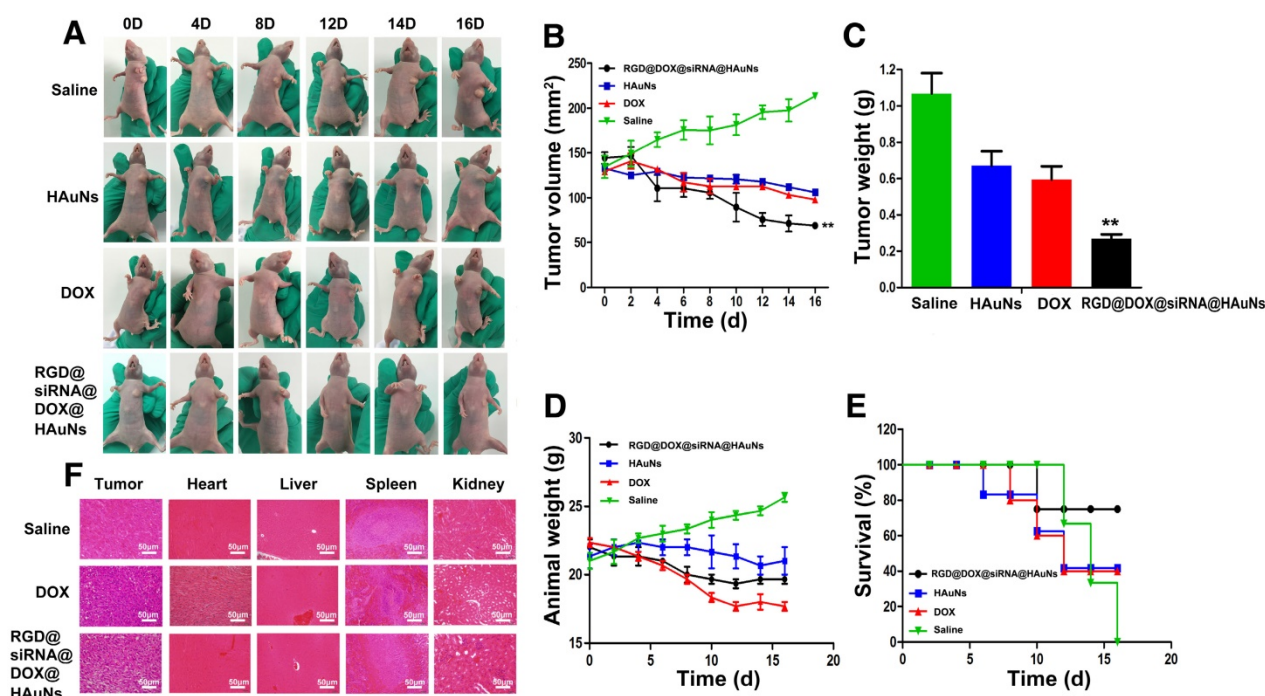


Figure 6. Antitumor therapeutic efficacy of RGD@DOX@siRNA@HAuNs on tumor-bearing mice. (A) Images of mice with tumors treated as indicated. (B) Tumor volumes of mice bearing H2228 tumors under different treatments as indicated. (C) Tumor weights of mice bearing H2228 tumors from the different treatment groups on the 16th day after injection. (D) Body weights of mice bearing H2228 tumors in the different groups. (E) The 16-day survival rates of mice after different administrations. F, Analysis of the experiment tumor bearing mice tissue. A, H&E stained images of tumor, heart, liver, spleen and kidney sections collected from different treatment groups. Data are given as mean \pm SD (n=5). *, P<0.05.

Conclusion

In this study, we designed and developed a drug carrier system RGD@DOX@siRNA@HAuNs targeted specifically for the treatment of EML4-ALK gene fusion NSCLC. The multiple impressive qualities of the new multidimensional nanoplatform includes the high drug loading rate, controlled drug release, and selective tumor targeting. The combination of gene therapy, chemotherapy and thermal therapy (siRNA, DOX, photothermal induced by free gold nanoshell) exhibited a cooperative effect that improved the treatment of EML4-ALK gene fusion NSCLC in vitro and in vivo. This study provides a promising strategy for the treatment EML4-ALK gene fusion NSCLC.

Supplementary Material

Supplementary figures and tables.

<http://www.thno.org/v08p2621s1.pdf>

Acknowledgments

The authors are grateful to Natural Science Foundation Committee of China (NSFC 81220108012, 61335007, 81371684, 81000666, 81171395 and 81328012) and Project Supported by the Natural Science Foundation of Jiangsu Province, China (BK20160751) for their financial support.

Competing Interests

The authors have declared that no competing interest exists.

References

- [1] Paz-Ares L. Beyond first-line NSCLC therapy: chemotherapy or erlotinib? *Lancet Oncol.* 2012; 13: 225-27.
- [2] Pallis A G, Serfass L, Dziadziusko R, van Meerbeeck JP, Fennell D, Lacombe D, et al. Targeted therapies in the treatment of advanced/metastatic NSCLC. *Eur J Cancer.* 2009; 45: 2473-87.
- [3] Soda M, Choi Y L, Enomoto M, Takada S, Yamashita Y, Ishikawa S, et al. Identification of the transforming EML4-ALK fusion gene in non-small-cell lung cancer. *Nature.* 2007; 448: 561-66.
- [4] Shaw A T, Yeap B Y, Mino-Kenudson M, Digumarthy SR, Costa DB, Heist RS, et al. Clinical features and outcome of patients with non-small-cell lung cancer who harbor EML4-ALK. *J Clin Oncol.* 2009; 27: 4247-53.
- [5] Wong D W, Leung E L, So K K, Tam IY, Sihoe AD, Cheng LC, et al. The EML4-ALK fusion gene is involved in various histologic types of lung cancers from nonsmokers with wild-type EGFR and KRAS. *Cancer.* 2009; 115: 1723-33.
- [6] Djalalov S, Beca J, Hoch J S, Krahn M, Tsao MS, Cutz JC, et al. Cost effectiveness of EML4-ALK fusion testing and first-line crizotinib treatment for patients with advanced ALK-positive non-small-cell lung cancer. *J Clin Oncol.* 2014; 32: 1012-19.
- [7] Kim H R, Kim W S, Choi Y J, Choi CM, Rho JK, Lee JC. Epithelial-mesenchymal transition leads to crizotinib resistance in H2228 lung cancer cells with EML4-ALK translocation. *Mol Oncol.* 2013; 7: 1093-102.
- [8] Zhang S, Wang F, Keats J, Zhu X, Ning Y, Wardwell SD, et al. Crizotinib-resistant mutants of EML4-ALK identified through an accelerated mutagenesis screen. *Chem Biol Drug Des.* 2011; 78: 999-1005.
- [9] Wu H, Zhao Y, Mu X, Wu H, Chen L, Liu W, et al. A silica-polymer composite nano system for tumor-targeted imaging and p53 gene therapy of lung cancer. *J Biomater Sci Polym Ed.* 2015; 26: 384-400.
- [10] Razi Soofiyani S, Kazemi Z, Lotfipour F, Mohammad Hosseini A, Shanehbandi D, Hallaj-Nezhadi S, et al. Gene therapy with IL-12 induced enhanced anti-tumor activity in fibrosarcoma mouse model. *Artif Cells Nanomed Biotechnol.* 2016; 44: 1988-93.

- [11] Kim SH, Jeong JH, Lee SH, Kim SW, Park TG. PEG conjugated VEGF siRNA for anti-angiogenic gene therapy. *J Control Release.* 2006; 116: 123-9.
- [12] Kim WJ, Chang CW, Lee M, Kim SW. Efficient siRNA delivery using water soluble lipopolymer for anti-angiogenic gene therapy. *J Control Release.* 2007; 118: 357-63.
- [13] Wu Y, Wang W, Chen Y, Huang K, Shuai X, Chen Q, et al. The investigation of polymer-siRNA nanoparticle for gene therapy of gastric cancer in vitro. *Int J Nanomedicine.* 2010; 5: 129-36.
- [14] Takezawa K, Okamoto I, Nishio K, Jänne PA, Nakagawa K. Role of ERK-BIM and STAT3-survivin signaling pathways in ALK inhibitor-induced apoptosis in EML4-ALK-positive lung cancer. *Clin Cancer Res.* 2011; 17: 2140-48.
- [15] Tanizaki J, Okamoto I, Okabe T, Sakai K, Tanaka K, Hayashi H, et al. Activation of HER family signaling as a mechanism of acquired resistance to ALK inhibitors in EML4-ALK-positive non-small cell lung cancer. *Clin Cancer Res.* 2012; 18: 6219-26.
- [16] Lee EJ, Gusev Y, Jiang J, Nuovo GJ, Lerner MR, Frankel WL, et al. Expression profiling identifies microRNA signature in pancreatic cancer. *Int J Cancer.* 2007; 120: 1046-54.
- [17] Lu Z, Li Y, Takwi A, Li B, Zhang J, Conklin DJ, et al. miR-301a as an NF-kappa B activator in pancreatic cancer cells. *EMBO J.* 2011; 30: 57-67.
- [18] Chen Z, Chen LY, Dai HY, Wang P, Gao S, Wang K. miR-301a promotes pancreatic cancer cell proliferation by directly inhibiting Bim expression. *J Cell Biochem.* 2012; 113: 3229-35.
- [19] Wu D, Chen B, Cui F, He X, Wang W, Wang M. Hypoxia-induced microRNA-301b regulates apoptosis by targeting Bim in lung cancer. *Cell Prolif.* 2016; 49: 476-83.
- [20] Stern JM, Kibanov Solomonov VV, Sazykina E, Schwartz JA, Gad SC, Goodrich GP. Initial Evaluation of the Safety of Nanoshell-Directed Photothermal Therapy in the Treatment of Prostate Disease. *Int J Toxicol.* 2016; 35: 38-46.
- [21] Luo H, Xu M, Zhu X, Zhao J, Man S, Zhang H. Lung cancer cellular apoptosis induced by recombinant human endostatin gold nanoshell-mediated near-infrared thermal therapy. *Int J Clin Exp Med.* 2015; 8: 8758-66.
- [22] Elliott AM, Shetty AM, Wang J, Hazle JD, Jason Stafford R. Use of gold nanoshells to constrain and enhance laser thermal therapy of metastatic liver tumors. *Int J Hyperthermia.* 2010; 26: 434-40.
- [23] Liu H, Chen D, Li L, Liu T, Tan L, Wu X, et al. Multifunctional Gold Nanoshells on Silica Nanorattles: A Platform for the Combination of Photothermal Therapy and Chemotherapy with Low Systemic Toxicity. *Angew Chem Int Ed Engl.* 2011; 50: 891-95.
- [24] Bardhan R, Lal S, Joshi A, Halas NJ. Theranostic Nanoshells: From Probe Design to Imaging and Treatment of Cancer. *Acc Chem Res.* 2011; 44: 936-46.
- [25] Braun GB, Pallaoro A, Wu G, Missirlis D, Zasadzinski JA, Tirrell M, et al. Laser-Activated Gene Silencing via Gold Nanoshell-siRNA Conjugates. *ACS Nano.* 2009; 3: 2007-15.
- [26] Huschka R, Barhoumi A, Liu Q, Roth JA, Ji L, Halas NJ. Gene silencing by gold nanoshell-mediated delivery and laser-triggered release of antisense oligonucleotide and siRNA. *ACS Nano.* 2012; 6: 7681-91.
- [27] Braun GB, Pallaoro A, Wu G, Missirlis D, Zasadzinski JA, Tirrell M, et al. Laser-Activated Gene Silencing via Gold Nanoshell-siRNA Conjugates. *ACS Nano.* 2009; 3: 2007-15.
- [28] Li J, Hu Y, Yang J, Wei P, Sun W, Shen M, et al. Hyaluronic acid-modified Fe₃O₄@Au core/shell nanostars for multimodal imaging and photothermal therapy of tumors. *Biomaterials.* 2015; 38: 10-21.
- [29] Hu Y, Wang R, Wang S, Ding L, Li J, Luo Y, et al. Multifunctional Fe₃O₄@Au core/shell nanostars: a unique platform for multimode imaging and photothermal therapy of tumors. *Sci Rep.* 2016; 6: 28325.
- [30] Li X, Xing L, Zheng K, Wei P, Du L, Shen M, et al. Formation of Gold Nanostar-Coated Hollow Mesoporous Silica for Tumor Multimodality Imaging and Photothermal Therapy. *ACS Appl Mater Interfaces.* 2017; 9: 5817-27.
- [31] Li X, Xing L, Hu Y, Xiong Z, Wang R, Xu X, et al. An RGD-modified hollow silica@Au core/shell nanoplatform for tumor combination therapy. *Acta Biomater.* 2017; 62: 273-83.
- [32] Ruifang Zhao, Xuexiang Han, Yiye Li, Hai Wang, Tianjiao Ji, Yuliang Zhao, et al. Photothermal Effect Enhanced Cascade-Targeting Strategy for Improved Pancreatic Cancer Therapy by Gold Nanoshell@Mesoporous Silica Nanorod. *ACS Nano.* 2017; 11: 8103-13.
- [33] Ma Y, Liang X, Tong S, Bao G, Ren Q, Dai Z. Gold Nanoshell Nanomicelles for Potential Magnetic Resonance Imaging, Light-Triggered Drug Release, and Photothermal Therapy. *Adv Fun Mater.* 2013; 23: 815-22.
- [34] Yang J, Lee J, Kang J, Oh SJ, Ko HJ, Son JH, et al. Smart drug-loaded polymer gold nanoshells for systemic and localized therapy of human epithelial cancer. *Adv Mater.* 2009; 21: 4339-42.
- [35] Jing L, Liang X, Li X, Lin L, Yang Y, Yue X, et al. Mn-porphyrin conjugated Au nanoshells encapsulating doxorubicin for potential magnetic resonance imaging and light triggered synergistic therapy of cancer. *Theranostics.* 2014; 11: 858-71.
- [36] Ke H, Wang J, Tong S, Jin Y, Wang S, Qu E, et al. Gold nanoshelled liquid perfluorocarbon magnetic nanocapsules: a nanotheranostic platform for bimodal ultrasound/magnetic resonance imaging guided photothermal tumor ablation. *Theranostics.* 2013; 1: 12-23.
- [37] Chen Q, Wang H, Liu H, Wen S, Peng C, Shen M, et al. Multifunctional dendrimer-entrapped gold nanoparticles modified with RGD peptide for

- targeted computed tomography/magnetic resonance dual-modal imaging of tumors. *Anal Chem.* 2015; 87: 3949-56.
- [38] Choi CH, Hao L, Narayan SP, Auyeung E, Mirkin CA. Mechanism for the Endocytosis of Spherical Nucleic Acid Nanoparticle Conjugates. *Proc Natl Acad Sci U S A.* 2013; 110: 7625-30.